Glucosyltransferase-dependent and independent effects of Clostridioides difficile toxins during infection

PLOS PATHOGENS

RESEARCH ARTICLE

Glucosyltransferase-dependent and independent effects of *Clostridioides difficile* toxins during infection

F. Christopher Peritore-Galve[1,2], John A. Shupe[1,2], Rory J. Cave[3], Kevin O. Childress[1,2], M. Kay Washington[1], Sarah A. Kuehne[4], D. Borden Lacy[1,2,5]*

1 Department of Pathology, Microbiology, and Immunology, Vanderbilt University Medical Center, Nashville, Tennessee, United States of America, **2** Vanderbilt Institute for Infection, Immunology, and Inflammation, Vanderbilt University Medical Center, Nashville, Tennessee, United States of America, **3** School of Biomedical Sciences, University of West London, London, United Kingdom, **4** Oral Microbiology Group, School of Dentistry and Institute of Microbiology and Infection, College of Medical and Dental Sciences, The University of Birmingham, Birmingham, United Kingdom, **5** Department of Veterans Affairs Medical Center, Nashville, Tennessee, United States of America

* borden.lacy@vumc.org

Citation: Peritore-Galve FC, Shupe JA, Cave RJ, Childress KO, Washington MK, Kuehne SA, et al. (2022) Glucosyltransferase-dependent and independent effects of *Clostridioides difficile* toxins during infection. PLoS Pathog 18(2): e1010323. https://doi.org/10.1371/journal.ppat.1010323

Editor: Theresa M. Koehler, University of Texas Medical School at Houston, UNITED STATES

Received: October 7, 2021

Accepted: January 30, 2022

Published: February 17, 2022

Data Availability Statement: All relevant data are within the manuscript and its Supporting Information files with the exception of genomic sequencing reads which are available on NCBI Sequencing Read Archive with the accession number PRJNA762329.

Funding: This project was supported by the funding from the National Institutes of Health (NIH) and the United States Department of Veterans Affairs (VA). FCPG was supported by NIH grant T32 DK007673, and DBL received funding through

Abstract

Clostridioides difficile infection (CDI) is the leading cause of nosocomial diarrhea and pseudomembranous colitis in the USA. In addition to these symptoms, patients with CDI can develop severe inflammation and tissue damage, resulting in life-threatening toxic megacolon. CDI is mediated by two large homologous protein toxins, TcdA and TcdB, that bind and hijack receptors to enter host cells where they use glucosyltransferase (GT) enzymes to inactivate Rho family GTPases. GT-dependent intoxication elicits cytopathic changes, cytokine production, and apoptosis. At higher concentrations TcdB induces GT-independent necrosis in cells and tissue by stimulating production of reactive oxygen species via recruitment of the NADPH oxidase complex. Although GT-independent necrosis has been observed *in vitro*, the relevance of this mechanism during CDI has remained an outstanding question in the field. In this study we generated novel *C. difficile* toxin mutants in the hypervirulent BI/NAP1/PCR-ribotype 027 R20291 strain to test the hypothesis that GT-independent epithelial damage occurs during CDI. Using the mouse model of CDI, we observed that epithelial damage occurs through a GT-independent process that does not involve immune cell influx. The GT-activity of either toxin was sufficient to cause severe edema and inflammation, yet GT activity of both toxins was necessary to produce severe watery diarrhea. These results demonstrate that both TcdA and TcdB contribute to disease pathogenesis when present. Further, while inactivating GT activity of *C. difficile* toxins may suppress diarrhea and deleterious GT-dependent immune responses, the potential of severe GT-independent epithelial damage merits consideration when developing toxin-based therapeutics against CDI.

NIH grant AI957555 and VA grant VA BX002943. The funders had no role in study design, data collection and analysis, decision to publish, or preparation of the manuscript.

Competing interests: The authors have declared that no competing interests exist.

Author summary

Clostridioides difficile is an anaerobic spore-forming bacterium that is the leading cause of antibiotic-associated diarrhea and pseudomembranous colitis in the USA. This pathogen produces two protein toxins, TcdA and TcdB, that enter host colon cells to cause inflammation, fluid secretion, and cell death. The enzymatic activity of TcdB is a target for novel *C. difficile* infection (CDI) therapeutics since it is considered the major factor in causing severe CDI. However, necrotic cell death due to non-enzymatic TcdB-host interactions has been reported in cell culture and colonic explant experiments. Here, we generated *C. difficile* mutant strains with enzyme-inactive toxins to evaluate each toxin's role in an animal model of CDI. We observe an additive role for TcdA and TcdB in disease, and both glucosyltransferase-dependent and independent phenotypes. These findings are expected to inform the development of toxin-based CDI therapeutics.

Introduction

Clostridioides difficile infection (CDI; formerly *Clostridium difficile*) is the leading cause of hospital-acquired diarrhea and pseudomembranous colitis in the USA [1,2]. *C. difficile* is a Gram-positive, spore-forming anaerobe that infects the colon, causing mild to severe symptoms including diarrhea, pseudomembranous colitis, toxic megacolon, and in severe cases, death [3]. CDI is prevalent among elderly and immunocompromised individuals in healthcare settings, typically following treatment with broad spectrum antibiotics. However, the rate of community-acquired infections among healthy individuals has increased over the past two decades due to the emergence of novel epidemic *C. difficile* strains [3,4]. Despite the clinical importance of CDI, we do not have a complete understanding of molecular host-microbe interactions during infection, which hinders our progress towards developing effective prevention and treatment strategies.

CDI is mediated by two large homologous protein toxins, TcdA (308 kDa) and TcdB (270 kDa) that are secreted during infection to cause disease symptoms. The toxins bind host cell receptors and become internalized into vesicles via endocytosis [5]. Endosome acidification elicits structural changes in the toxins, stimulating pore formation and translocation of the N-terminal glucosyltransferase (GT) and autoprocessing (AP) domains into the cytosol [5]. Inositol-6-phosphate-induced autoprocessing releases the GT domain in the host cell and permits access to Rho family GTPases. GT activity transfers glucose from UDP-glucose onto Rho GTPases, irreversibly inactivating these regulatory proteins [5–8]. This inactivation causes cytoskeletal rearrangement, leading to the disruption of cell adhesion junctions, cytopathic changes, and apoptosis [5]. These effects stimulate proinflammatory cytokines and neutrophil chemoattractants that generate acute inflammatory responses. Prolonged host inflammation during CDI increases the severity of tissue damage and the probability of lethal disease outcomes [9–11].

In addition to GT-dependent effects of *C. difficile* toxins, TcdB can induce GT-independent necrotic cell death at high concentrations *in vitro* (> 0.1 nM) [12,13]. This effect occurs through the stimulation of reactive oxygen species via the NADPH oxidase complex [14]. In contrast, TcdA induces GT-dependent cell death through the apoptosis pathway at both high and low concentrations [15]. TcdA and TcdB can also stimulate cytokine release *in vitro* through both GT-dependent and independent pathways [9]. The relevance of GT-independent cell death during infection has been unclear since it is unknown if cells encounter the concentration of TcdB required to stimulate necrotic cell death. A recent study concluded that GT

activity was necessary to cause CDI in mouse and hamster models of infection, but this does not preclude an additional role for GT-independent events as the infection progresses [16]. The study also involved GT-defective *C. difficile* mutants in the 630 strain, which is genetically tractable, but causes only mild disease symptoms in animal models [17]. In contrast, the BI/NAP1/PCR-ribotype 027 epidemic strains have been associated with multiple human epidemics and cause significant pathology in animal models of infection [16–19]. Among several differences, the 630 strain has been characterized as one with low expression levels of TcdA and TcdB [17,19].

Historically, TcdA was considered the toxin responsible for CDI pathogenesis [20]. The identification of patient-derived clinical isolates that are TcdA-negative and TcdB-positive, along with functional analyses of toxin mutants in animal models indicated however that TcdB is necessary and sufficient to cause severe CDI [21,22]. Other data demonstrate that TcdA alone can cause symptoms in the hamster model of infection, suggesting a role for both toxins during disease [23]. Overall, the respective roles of TcdA and TcdB during infection are not fully understood.

CDI remains a pervasive disease across the world and poses a significant burden on patients and the healthcare system. The main goal of this study was to define GT-dependent and independent effects of each toxin during CDI using the mouse model of infection and a BI/NAP1/PCR-ribotype 027 epidemic strain. The results from this study provide a framework to further understand the complex molecular interplay between *C. difficile* toxins and the host colon during infection.

Results

Generation of glucosyltransferase-deficient mutants and *in vitro* characterization

To define GT-dependent and independent effects of TcdA and TcdB during infection, GT-deficient mutants were generated in the epidemic *C. difficile* BI/NAP1/PCR-ribotype 027 R20291 background (hereafter referred to as R20291) using homologous allelic exchange [24]. This approach allowed for the introduction of single nucleotide mutations (SNMs) in the GTD of either or both toxins, causing single point mutations at positions TcdA::D285N/D287N and/or TcdB::D286N/D288N (Fig 1A). Four novel mutant strains were created, including GT-deficient mutants for each toxin (A_{GTX} B+ and A+ B_{GTX}), a GT-deficient mutant of both toxins (A_{GTX} B_{GTX}), and a total *tcdA* knockout with GT-deficient TcdB (Δ*tcdA* B_{GTX}) (Table 1). Whole genome sequencing was performed on all strains used in this study to ensure the proper mutations were present and that there were no off-target mutations that might affect their phenotypes (Table 1 and Fig 1A) [25]. There were no unexpected variations in nucleotides for any of the mutant strains compared to the wildtype background and the reference R20291 genome (NC_013316). All sequencing reads are available in the NCBI Sequencing Read Archive under accession number PRJNA762329.

The novel strains were tested for toxin secretion and bacterial growth *in vitro* to ensure that the introduced mutations had no unintended effects on these processes. Toxin secretion was determined in mutant and wildtype strains cultured for 24 hours in toxin-inducing TY medium. After 24 hours of growth, cell pellets and supernatants were separated by centrifugation, then supernatants were filter-sterilized to remove any cell contaminants. Immunoblot analyses of TcdA and TcdB determined that there were no GT-dependent effects on toxin secretion and confirmed the knockout phenotypes of Δ*tcdA* B_{GTX} and Δ*tcdA* Δ*tcdB* (Fig 1B). *In vitro* growth of each strain was assessed in BHIS medium for 24 hours under anaerobic conditions. Bacterial growth was measured every hour, revealing that there were no significant differences in growth between mutant and wildtype strains (Fig 1C).

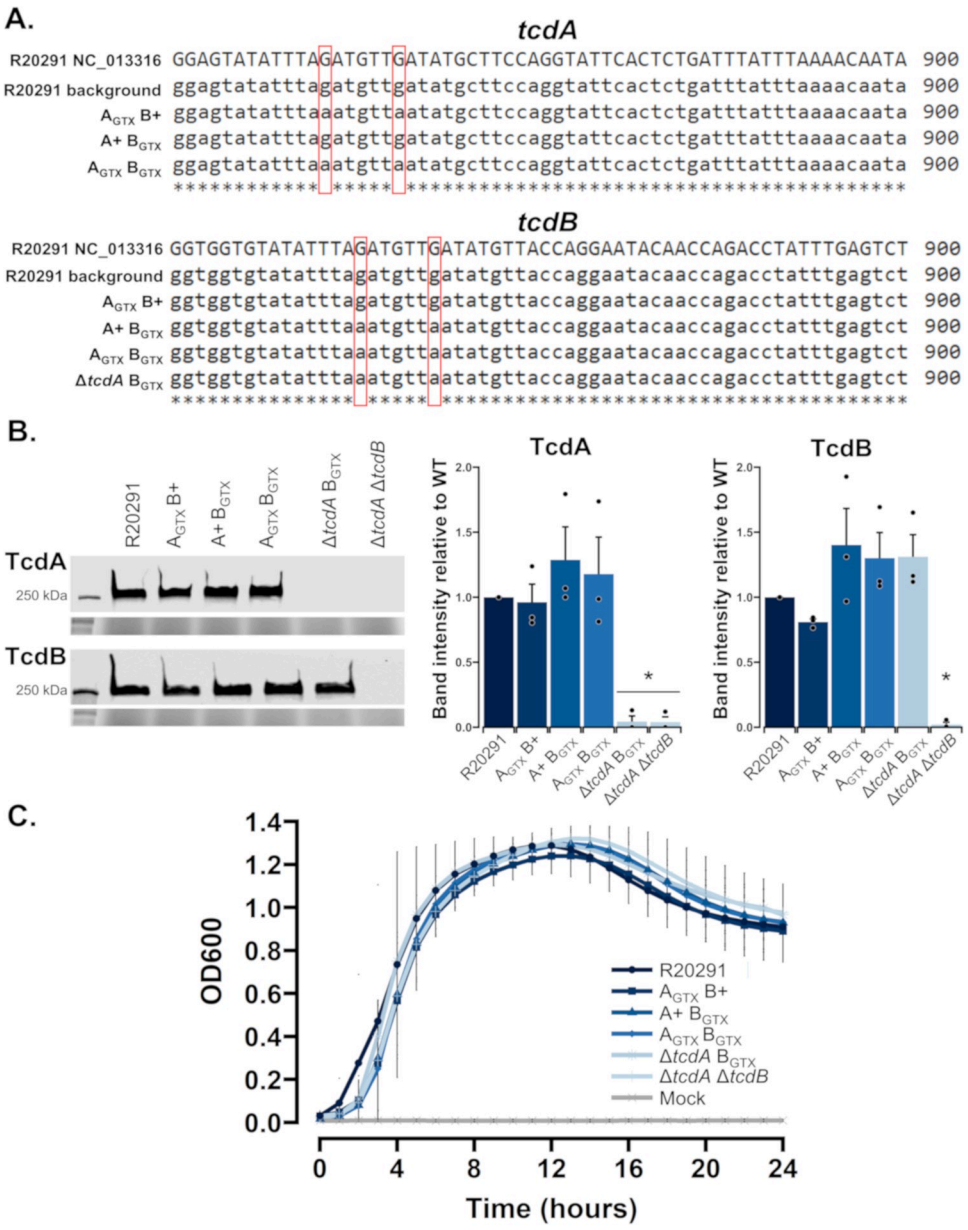

Fig 1. In vitro characterization of *C. difficile* mutants. (A) *tcdA* and *tcdB* gene alignments of mutant and wildtype strains to the reference genome of R20291. Red boxes highlight SNMs that deactivate GT catalytic activity. (B) Representative Western blot images of mutant and wildtype strains to confirm secretion (or lack thereof) of TcdA and TcdB. Images directly below each Western blot are stain-free gel images shown as loading controls. The graphs show densitometry analyses from Western blot experiments ($n = 3$). Dots signify each replicate, bars denote the mean, and error bars represent the standard error of the mean. Significant differences were determined by Tukey's HSD (* $p < 0.05$). (C) *In vitro* growth curves of each strain and mock-inoculated controls ($n = 5$ per treatment) cultured in BHIS for 24 hours. Dots are the average at each given timepoint, and the error bars depict the 95% confidence interval.

https://doi.org/10.1371/journal.ppat.1010323.g001

Finally, we confirmed mutant and wildtype toxin function *in vitro* using cell rounding assays. Strain supernatants were obtained from bacteria cultured in toxin-inducing TY medium, followed by centrifugation and filter sterilization to remove cell contaminants. Dilutions of strain supernatants, TY, and purified recombinant TcdA (100 pM) and TcdB (1 pM) were placed into individual wells each containing 20,000 Vero cells and cytopathic rounding

Table 1. Strains and plasmids used in this study.

Strains	Description	Source or Citation
Clostridioides difficile		
R20291Δ*pyrE*	Wildtype BI/NAP1/PCR-ribotype 027 strain obtained from CRG0825 stock at the Nottingham Clostridia Research Group, Cardiff, UK with *pyrE* knocked out.	[24]
R20291	Wildtype BI/NAP1/PCR-ribotype 027 strain obtained from CRG0825 stock at the Nottingham Clostridia Research Group, Cardiff, UK with restored *pyrE*.	[24]
A_{GTX} B+	R20291 TcdA::D285N/D287N	This study
A+ B_{GTX}	R20291 TcdB::D286N/D288N	This study
A_{GTX} B_{GTX}	R20291 TcdA::D285N/D287N-TcdB::D286N/D288N	This study
Δ*tcdA* B_{GTX}	R20291 Δ*tcdA* TcdB::D286N/D288N	This study
Δ*tcdA* Δ*tcdB*	R20291 *tcdA/tcdB* ClosTron insertional mutants	[47]
Escherichia coli		
DH5α	Chemically competent *E. coli* cells for transformation	NEB
CA434	Conjugation host	[37]
Plasmids	**Description**	**Source or Citation**
pMTL-YN4	Knockout vector for R20291	[24]
pMTL-YN4::TcdA	KO vector backbone with 2393 bp fragment of *tcdA* GTD	This study
pMTL-YN4::TcdB	KO vector backbone with 2332 bp fragment of *tcdB* GTD	This study
pMTL-YN4::TcdA D285N/D287N	KO vector backbone with mutations in *tcdA*	This study
pMTL-YN4::TcdB D286N/D288N	KO vector backbone with mutations in *tcdA*	This study
pMTL-YN4::TcdA KO	KO vector backbone with left flank and right flanks of *tcdA* for full gene deletion	This study

https://doi.org/10.1371/journal.ppat.1010323.t001

was imaged every hour. This experiment confirmed that cell rounding required functional TcdA, TcdB or both toxins (S1 Fig). Consistent with previously published data, TcdB demonstrated faster kinetics of rounding compared to TcdA (S1 Fig). Validation of mutant genotypes, toxin secretion, bacterial growth, and toxin function allowed us to confidently move into animal infection experiments.

Glucosyltransferase activity of both toxins causes the most severe disease outcomes

The non-lethal mouse model of infection was used to define GT-dependent and independent effects of each toxin during CDI. Mice were pre-treated with cefoperazone antibiotics in drinking water for five days, then were returned to regular drinking water for two days prior to inoculation with *C. difficile* (Fig 2A). *C. difficile* spores of each strain (10^5 CFU/mL) were administered via oral gavage, and metrics of infection and symptom severity were assessed daily until 2- or 4-days post-inoculation (dpi). The most severe decline in animal weight occurred at 2 dpi, then mice began to recover by 4 dpi (Fig 2B). Thus, the starkest differences between treatments were observed at 2 dpi (S2 Fig). At 2 dpi, the wildtype R20291 strain induced 12% weight loss on average, which was significantly more than all other groups, even when compared to A_{GTX} B+ ($p = 0.0075$) and A+ B_{GTX} ($p < 0.0001$) (Figs 2B and S2). A_{GTX} B+ caused the second highest average weight loss at 2 dpi (8.9%), but was not significantly different from A+ B_{GTX}, which caused 6.4% average weight loss ($p = 0.2273$; Figs 2B and S2).

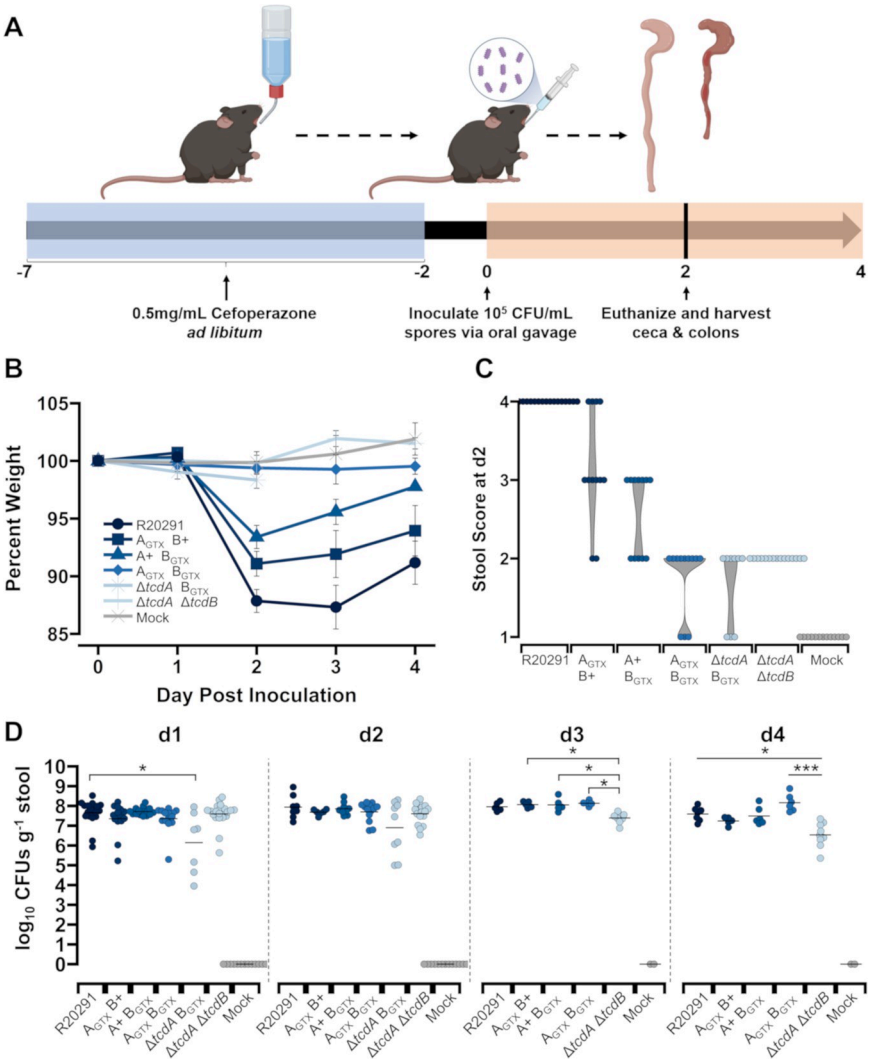

Fig 2. GT-dependent and independent effects on weight loss, diarrhea, and colonization in the mouse model of *C. difficile* infection. (A) Visual abstract of the cefoperazone mouse model of CDI used for this study. The figure was created with BioRender (B) Percent weight loss from day 0 for R20291 ($n = 22$), A_{GTX} B+ ($n = 15$), A+ B_{GTX} ($n = 15$), A_{GTX} B_{GTX} ($n = 15$), Δ*tcdA* B_{GTX} ($n = 9$), Δ*tcdA* Δ*tcdB* ($n = 22$), and mock ($n = 13$). Points represent group averages at each day and error bars denote standard error of the mean. (C) Stool scores at 2 dpi. (D) Daily *C. difficile* burden in stool. Each point is an individual mouse, and the crossbars represent group daily means. Significantly different groups as determined by Dunn's test are shown in brackets (* $p < 0.05$; *** $p < 0.001$).

https://doi.org/10.1371/journal.ppat.1010323.g002

Mice inoculated with A_{GTX} B_{GTX}, Δ*tcdA* B_{GTX}, Δ*tcdA* Δ*tcdB*, or mock (sterile PBS) lost little to no weight (Figs 2B and S2). Similar trends between treatments were observed at 3 and 4 dpi (Figs 2B and S2).

Weight loss is typically caused by increased fluid loss during CDI-associated diarrhea. To visually test the effects of GT activity of each toxin on diarrhea severity, mouse stool was collected daily for visual assessment of moisture, color, and consistency. Stool scores from 1-to-4 were assigned based on pre-defined criteria. All mice inoculated with wildtype R20291 had a stool score of 4 at 2 dpi based on the presence of watery diarrhea and wet tail (Fig 2C). Although some mice inoculated with A_{GTX} B+ developed severe watery diarrhea, most had a stool score of 3, characterized by soft and discolored stool (Fig 2C). No mice inoculated with A + B_{GTX} developed watery diarrhea, and typically displayed soft, discolored stool (Fig 2C). Stool

from mutant strains that induced no weight loss (A_{GTX} B_{GTX}, Δ*tcdA* B_{GTX}, and Δ*tcdA* Δ*tcdB*) was well formed, yet discolored (Fig 2C).

To quantify *C. difficile* burden during infection, daily fecal samples were collected, weighed, homogenized, then dilution plated onto semi-selective media. At 1 dpi, strains colonized to a high density (~10^7 CFU g^{-1} stool), however, R20291 was significantly more abundant in stool compared to Δ*tcdA* B_{GTX} ($p = 0.031$; Fig 2D). There were no significant differences in *C. difficile* stool burden between strains at 2 dpi, when symptoms were most severe. Colonization density of Δ*tcdA* Δ*tcdB* began to significantly reduce at 3 and 4 dpi, while titers of other strains remained more consistent. As expected, no mock-inoculated mice contained *C. difficile* (Fig 2D). Since there were no notable differences in *C. difficile* burden in stool, it is expected that symptom severity phenotypes caused by each strain are due to molecular toxin-host interactions and not colonization burden.

Edema and inflammation are glucosyltransferase-dependent, but epithelial damage is glucosyltransferase-independent

To visualize diarrhea and inflammation on a macroscale, mice were euthanized at 2 dpi, then ceca and colons were excised and imaged ($n = 6$ per treatment). The ceca and colons of mice inoculated with the wildtype R20291 strain were severely inflamed and contained very little wet stool (Fig 3A). Soft, discolored stool was typically observed in ceca and colons from mice inoculated with A_{GTX} B+ and A+ B_{GTX} (Fig 3A). Stool discoloration from A_{GTX} B_{GTX}, Δ*tcdA* B_{GTX}, and Δ*tcdA* Δ*tcdB*-inoculated mice was noted in ceca and colons, relative to well-formed, normal colored stool from mock-inoculated mice (Fig 3A).

Whole organ inflammation was determined by measuring cecum area and colon length (Fig 3B). The area of ceca from mice inoculated with R20291, A_{GTX} B+, and A+ B_{GTX} were half the size of those from mice inoculated with A_{GTX} B_{GTX}, Δ*tcdA* B_{GTX}, Δ*tcdA* Δ*tcdB*, and the mock control ($p < 0.001$; Fig 3B). Colon length was altered in response to weight loss-inducing strains, albeit less drastically than differences observed in ceca (Fig 3B). Colons from mice inoculated with R20291, A_{GTX} B+, and A+ B_{GTX} were significantly shorter than mock-inoculated mice ($p < 0.05$; Fig 3B). However, none were significantly shorter than mice inoculated with Δ*tcdA* Δ*tcdB* ($p > 0.05$; Fig 3B).

To examine histopathological phenotypes in infected tissues, excised ceca were fixed and frozen in OCT media, then cryosectioned and H&E stained. Edema, inflammation, and epithelial damage were scored on a 1–4 scale by a board-certified gastrointestinal pathologist based on previously published criteria [18]. Cecal edema was observed in mice inoculated with R20291, A_{GTX} B+, and A+ B_{GTX}, and was scored on average between 2 and 3 based on the presence of moderate to severe edema with widespread multifocal submucosal expansion ($p < 0.001$; Fig 3C and 3D) [18].

Phenotypes of cecal inflammation were more nuanced than edema. Once again, R20291, A_{GTX} B+, and A+ B_{GTX}, caused the highest average inflammation scores (2–3), hallmarked by moderate to severe neutrophilic inflammation and submucosal to mural involvement ($p < 0.001$; Fig 3C and 3D) [18]. However, A_{GTX} B_{GTX} caused minimal to moderate inflammation and did not significantly differ from inflammation induced by A+ B_{GTX} ($p = 0.1736$; Fig 3C and 3D).

Finally, epithelial damage was assessed. Severe epithelial damage was observed in mice inoculated with R20291, A_{GTX} B+, A+ B_{GTX}, and A_{GTX} B_{GTX} (Fig 3C and 3D). Mice with epithelial damage scores between 3–4 exhibited severe multifocal epithelial vacuolation, apoptotic figures, and severely damaged regions developed pseudomembranes (Figs 3D and 4) [18]. Minimal epithelial damage was observed in Δ*tcdA* B_{GTX}, Δ*tcdA* Δ*tcdB*, or mock-inoculated mice (Figs 3D and 4).

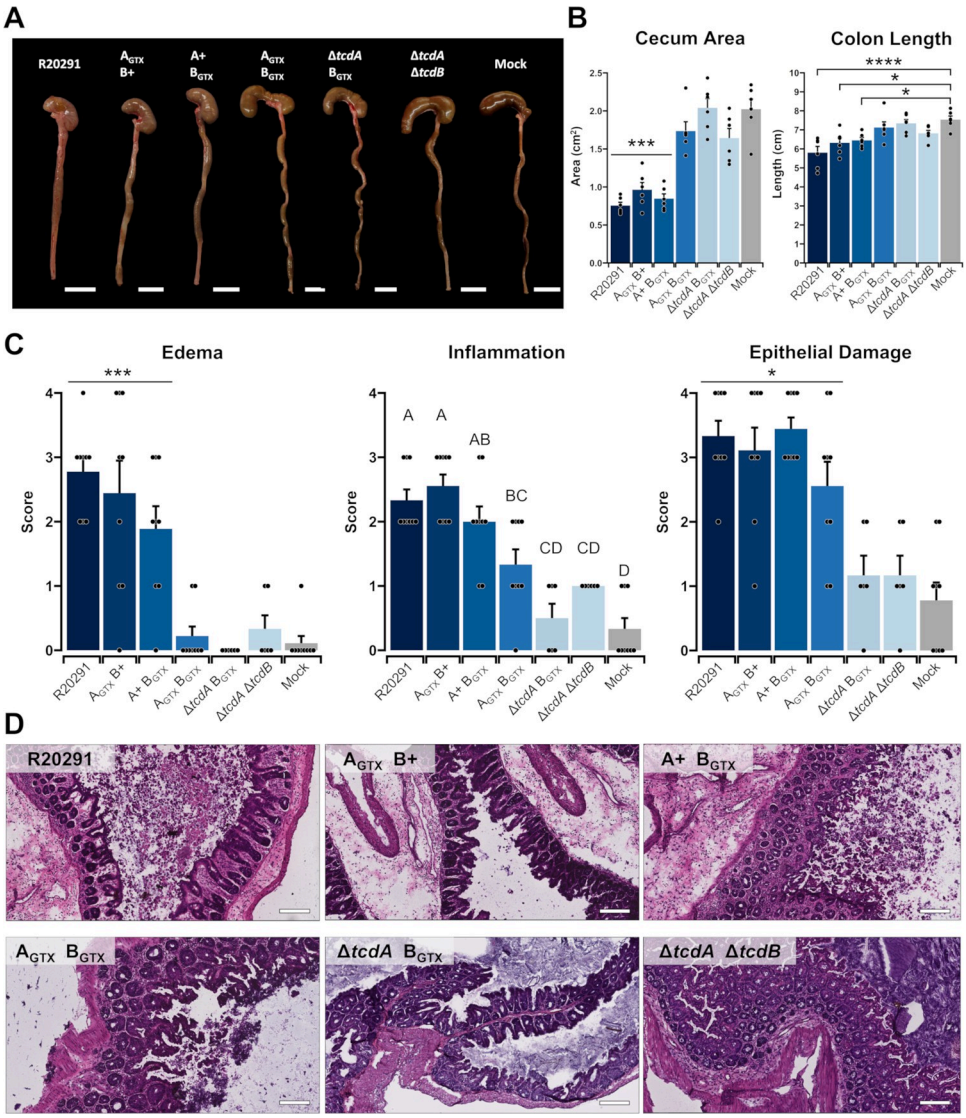

Fig 3. Glucosyltransferase activity causes edema and inflammation, but epithelial damage is glucosyltransferase independent. (A) Representative images of ceca and colons from mice inoculated with each treatment at 2 dpi. White bars denote 1 cm. (B) Cecum area and colon length as metrics of organ inflammation. Bars are the mean of each group and points are individuals within the group. Error bars represent standard error of the mean. Differences in cecum area depict that R20291, A_{GTX} B+, and A+ B_{GTX} are significantly smaller than the four other groups. Differences in colon length are comparing R20291, A_{GTX} B+, and A+ B_{GTX} to mock-inoculated colons. (C) Epithelial damage, inflammation, and edema mean scores as determined by a gastrointestinal pathologist. Points represent each individual animal and error bars are the standard error of the mean ($n = 6–9$ per treatment). Statistical differences as determined by Tukey's HSD are shown in brackets (* $p < 0.05$; *** $p < 0.001$; **** $p < 0.0001$) or by letters ($p < 0.05$). (D) Representative H&E images of mouse ceca inoculated with each strain at 2 dpi. Scale bar, 80 μm.

https://doi.org/10.1371/journal.ppat.1010323.g003

Glucosyltransferase activity of TcdB is required to elicit MPO^+ immune cell infiltration

Epithelial damage can be induced or exacerbated by immune cell infiltrates, and pseudomembranes are often formed by sloughed epithelial cells and intraluminal neutrophils bound in a fibrinous matrix [18,26]. Therefore, immunohistochemical analyses of infected cecal tissues was employed to test GT-dependent effects on MPO^+ immune cell recruitment, and to

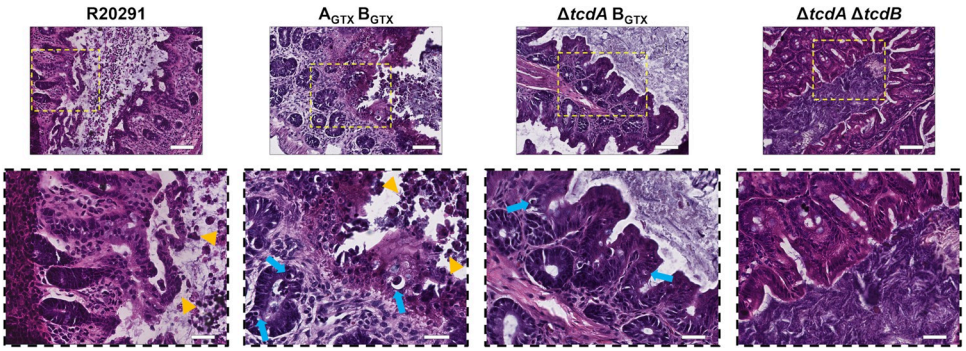

Fig 4. Epithelial damage is elicited by a glucosyltransferase-independent mechanism during infection. Representative images of severe epithelial injury in R20291 and A_{GTX} B_{GTX} compared to Δ*tcdA* B_{GTX} and Δ*tcdA* Δ*tcdB*. Scale bar, 80 μm in 20x magnification images. Zoomed in (40x magnification; dashed boxes) images offer a closer view at specific epithelial damage phenotypes. Apoptotic bodies or dying cells are highlighted by blue arrows. Sloughing dead cells and pre-pseudomembrane formation is shown by orange arrowheads. Scale bar, 130 μm.

https://doi.org/10.1371/journal.ppat.1010323.g004

determine if epithelial damage observed in A_{GTX} B_{GTX}-infected mice occurred through toxin-host interactions or aggressive immune cell infiltration. The number of MPO^+ cells per 20x field of view were quantified in single mucosal layers ($n = 3$ animals per treatment). This approach revealed that R20291 and A_{GTX} B+ caused the most significant immune cell influx during disease (~230 cells per FOV; $p < 0.001$; Fig 5). Although A+ B_{GTX} elicited mild MPO^+ cell recruitment, it was not significantly higher than that observed in mock-inoculated mice ($p = 0.2587$; Fig 5). Finally, A_{GTX} B_{GTX} caused considerable epithelial damage and pseudo-membrane formation, but there were few MPO^+ immune cells recruited to sites of epithelial damage (Fig 5).

Discussion

CDI continues to be a significant nosocomial disease in the USA and worldwide, and a more thorough understanding of the function of TcdA and TcdB during infection may open new

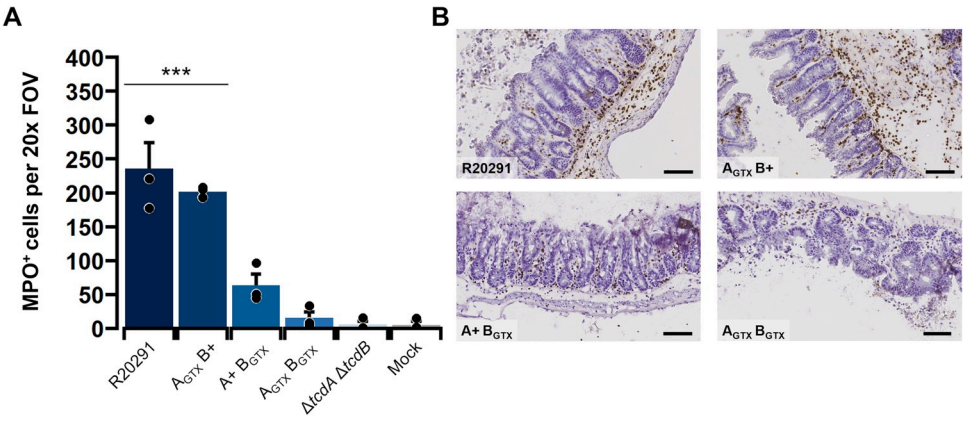

Fig 5. Glucosyltransferase activity of TcdB is required to elicit acute myeloperoxidase-positive immune cell infiltration. (A) Number of MPO^+ cells per single mucosal layer per 20x field of view (FOV). Each point is the average of three 20x FOVs from one animal. Bars depict the group mean and error bars are the standard error of the mean. Statistical differences between R20291 and A_{GTX} B+ and the other treatments as determined by Tukey's HSD are shown in a bracket (*** $p < 0.001$). (B) Representative MPO immunohistochemistry images showing high amounts of immune cell influx into submucosal and mucosal layers in R20291 and A_{GTX} B+, and lower amounts in A+ B_{GTX} and A_{GTX} B_{GTX}. Scale bar, 80 μm.

https://doi.org/10.1371/journal.ppat.1010323.g005

avenues for prevention and treatment therapies. This includes the development of toxin-inhibiting drugs such as small molecule inhibitors or neutralizing antibodies and nanobodies [19]. These compounds are designed to inhibit specific toxin domains such as the GTD, APD, or the combined oligopeptide repeat (CROPS) domain [5,19]. In recent years, efforts have focused on inhibiting the GT activity of TcdB since TcdB is considered the major driver of severe CDI symptoms. While conceptually an ideal target, multiple investigators have noted that glucosyltransferase-deficient toxin mutants are still cytotoxic or capable of eliciting cytokine responses [9,12–14,27,28].

The role of glucosyltransferase-independent activities during infection are not fully understood. Previous attempts to recapitulate GT-independent effects in murine models have included instillation of recombinant GT-defective TcdB by intrarectal instillation or cecal injection [29,30]. These studies found no GT-independent effects. However, these systems may have lacked the sensitivity of the *C. difficile* infection model, in which toxins are constantly produced and interact with the host epithelium over a course of several days. Recently, GT activity of TcdB was shown to be necessary to cause CDI, and there were no observed GT-independent effects in the mouse model of infection using defined GTX mutants in the *C. difficile* 630 strain [16]. This study had two limitations: the first being that the *C. difficile* 630 strain produces few CDI symptoms in the mouse model of infection when compared to epidemic *C. difficile* strains, and it also does not cause epithelial damage [16–18]. The second limitation was that histopathology was assessed at 5 dpi, a timepoint in which mice begin to recover from CDI [16,18]. The aim of our study was to define the GT-dependent and independent effects of *C. difficile* toxins during CDI using the epidemic BI/NAP1/PCR-ribotype 027 R20291 strain in the mouse model of infection and to look for evidence of epithelial damage at the time when weight loss is most severe.

In recent years, TcdB has been accepted as the main virulence factor necessary for fulminant CDI [21,22]. However, TcdA alone can cause mild to moderate CDI symptoms in animal models of infection [21–23]. In this study, mice were inoculated with novel isogenic mutants with deactivated GTDs of either or both toxins, as well as wildtype, double toxin KO, and mock-inoculated controls. The result of these experiments demonstrated that GT activity of TcdA or TcdB alone can cause moderate weight loss during infection, and that GT activity is required for CDI-induced weight loss. Mice inoculated with the wildtype R20291 strain lost the most weight, indicating that the toxins had an additive effect in causing the most severe weight loss outcomes. Additionally, the size of colons and ceca were measured, revealing that GT activity of either toxin was sufficient to cause significant inflammation and subsequent size reduction of both organs. Unexpectedly, we observed that R20291 was the only strain capable of causing severe watery diarrhea, whereas A+ B_{GTX} and A_{GTX} B+ only caused stool to become softer and discolored. Collectively, these results highlight the nuanced and additive effects of each toxin to CDI symptoms including weight loss, diarrhea, and organ inflammation.

Histological damage was assessed in mouse ceca, which is the site of the most severe histopathology in the mouse model of CDI [18]. Strains that had functional GT activity of one or both toxins caused severe multifocal edema, whereas GT-inactive or toxin knockout strains caused little to no edema. Inflammation was the most severe in mice inoculated with R20291, A_{GTX} B+, and A+ B_{GTX}. However, the severity of inflammation between A+ B_{GTX} and A_{GTX} B_{GTX} was not significantly different, suggesting a mild GT-independent effect on inflammation during infection. Wildtype R20291, A_{GTX} B+, A+ B_{GTX}, and A_{GTX} B_{GTX} all caused severe epithelial damage during infection. This phenotype was observed as dead and dying cells sloughing off into the lumen, and by the presence of pseudomembranes. Unexpectedly, Δ*tcdA* B_{GTX} did not elicit epithelial damage different from the double KO and mock controls, which may indicate that GT-independent effects of TcdA are necessary to potentiate epithelial

damage during CDI. Indeed, both TcdA and TcdB cause GT-independent effects on immune responses during intoxication *in vitro* and *in vivo* which may synergize to increase the severity of epithelial damage [9,27,31]. Together, these results demonstrate that edema and inflammation are GT-dependent and are elicited by TcdA or TcdB during infection, although mild inflammation can be caused in a GT-independent manner. They also indicate that epithelial injury occurs through GT-independent mechanisms of TcdA and TcdB during infection.

Since inflammation can contribute to epithelial damage in some models [26,32–35], immunohistochemical analyses were used to quantify GT-dependent and independent effects on MPO^+ immune cell influx. Strikingly, high amounts of MPO^+ cell infiltration were detected in mice inoculated with only R20291 or A_{GTX} B+. In contrast, relatively low levels of MPO^+ cells were observed in ceca from mice inoculated with A+ B_{GTX} and A_{GTX} B_{GTX} despite their induction of epithelial injury and inflammation. These results indicate that MPO^+ immune cell infiltration is dependent on GT activity of TcdB, and that A_{GTX} B_{GTX} causes severe epithelial damage and pseudomembrane formation in the absence of MPO^+ immune cell recruitment.

In conclusion, our data demonstrate that GT activity of either TcdA and TcdB is required for weight loss and organ inflammation, but GT activity of both toxins together causes the most severe weight loss and diarrhea phenotypes. Histological assessment of infected tissues revealed that GT activity of TcdA or TcdB can cause significant edema and inflammation, however GT-activity was not necessary to cause epithelial damage and pseudomembrane formation. Finally, analysis of MPO^+ immune cell recruitment demonstrated that GT activity of TcdB was required to elicit MPO^+ immune cells to sites of infection and that GT-independent epithelial damage did not require or elicit MPO^+ immune cell influx.

While we have observed GT-independent effects during infection, it is possible that therapeutic approaches targeting the GTD will be successful to halt downstream GT-dependent diarrhea and acute inflammatory responses that exacerbate disease severity. However, we must consider that there may be consequences from GT-independent epithelial damage and pseudomembrane formation that might occur when GT activity is neutralized, such as effects on CDI recurrence and/or colon-related diseases. Future studies will aim to elucidate these effects.

Materials and methods

Ethics statement

This study was approved by the Institutional Animal Care and Use Committee at Vanderbilt University Medical Center (VUMC) and performed using protocol M1700185-01. Our laboratory animal facility is AAALAC-accredited and adheres to guidelines described in the Guide for the Care and Use of Laboratory Animals. The health of the mice was monitored daily, and severely moribund animals were humanely euthanized by CO_2 inhalation followed by cervical dislocation. All animals in this study were C57BL/6J female mice between 8–10 weeks of age purchased from Jackson Laboratories. Mice were assimilated to the new facility for one week prior to antibiotic treatment to reduce stress. Mice were housed in a pathogen-free room with 12-hour cycles of light and dark. Cages were changed every two weeks to ensure clean bedding, and they had free access to food and water.

C. difficile culturing and spore generation

C. difficile strains were routinely cultured at 37˚C in brain-heart-infusion medium supplemented with 0.5% yeast extract and 0.1% cysteine (BHIS) in an anaerobic chamber (90% nitrogen, 5% hydrogen, 5% carbon dioxide). Strains were stored at -80˚C in 20% glycerol for long-term use.

Spores were prepared by transferring a single colony of each strain into 2 mL of BHIS and incubating overnight. The next day, the 2 mL culture was inoculated into 50 mL of Clospore medium, which was then grown for 10 days anaerobically [36]. After sporulation, the suspension was centrifuged at 4,000 x g at 4˚C and washed five times in cold sterile water. Spores were suspended in 1 mL sterile water and heat treated at 65˚C for 20 minutes to eliminate vegetative cells. Viable spores were quantified through serial dilutions and spotting on BHIS + 0.1% taurocholate (TA) plates. Spore stocks were stored at 4˚C until use.

C. difficile mutant generation

To study GT-dependent and independent effects during infection, *C. difficile* strains with mutations deactivating the GT catalytic domain ("GTX") of TcdA (TcdA::D285N/D287N), TcdB (TcdB::D286N/D288N), or both toxins (TcdA::D285N/D287N-TcdB::D286N/D288N) were generated (Table 1). Mutations were introduced in *tcdA* and *tcdB* genes of the BI/NAP1/PCR-ribotype 027 epidemic *C. difficile* R20291 strain using homologous allelic exchange [24]. Four novel strains were generated for this study: A_{GTX} B+, A+ B_{GTX}, A_{GTX} B_{GTX}, and Δ*tcdA* B_{GTX} (Table 1).

Mutants with deactivated catalytic domains were created by PCR amplifying a 2393 bp fragment of *tcdA*, and a 2332 bp fragment of *tcdB* from *C. difficile* R20291 genomic DNA (gDNA), then cloning amplicons into separate pMTL-YN4 vectors at flanking *AscI* and *SbfI* restriction sites [24].SNMs in *tcdB* were generated using Q5 Site-Directed Mutagenesis according to manufacturer's protocol (New England Biolabs). Briefly, oligonucleotides that contained the SNMs were used to PCR amplify the entire pMTL-YN4::*tcdB* vector (7788 bp), then treated with Kinase-Ligase-*DpnI* (New England Biolabs) prior to heat shock transformation into chemically competent DH5α *Escherichia coli* cells (Tables 1 and 2). Q5 Site-Directed Mutagenesis did not work for *tcdA*; therefore, Gibson assembly was used as an alternative approach. Each half of the pMTL-YN4::*tcdA* vector (7816 bp total) was amplified in two separate reactions using oligonucleotides containing SNMs in the overlap region to generate the SNMs in *tcdA* (Table 2). Finally, to generate the *tcdA* knockout (KO) cassette, *C. difficile* R20291 gDNA was PCR amplified with oligonucleotides flanking the *tcdA* gene that include the start and stop codons (Table 2). To create a whole-gene deletion, left and right homology arms (1039 bp and 1017 bp, respectively) of the amplified *tcdA* were created and joined together by Gibson assembly into the pMTL-YN4 plasmid at *AscI* and *SbfI* restriction sites to create pMTL-YN4::Δ*tcdA*, which was introduced into DH5α *E. coli* via heat shock (Tables 1 and 2) [24].

E. coli containing pMTL-YN4::*tcdA*, pMTL-YN4::*tcdB*, or pMTL-YN4::Δ*tcdA* were conjugated into a *C. difficile* R20291Δ*pyrE* mutant strain as previously described (Table 1) [24,37]. Transconjugants were selected based on thiamphenicol (15 μg/mL) resistance on BHIS plates supplemented with D-cycloserine (250 μg/mL) and cefoxitin (8 μg/mL) [24]. Single crossover integrants that were thiamphenicol resistant were further identified by PCR amplification and Sanger sequencing. Confirmed single cross-over clones were grown on BHIS supplemented with 500 μg/mL 5-fluoroorotic acid and 1 μg/mL uracil to induce *pyrE*-based counter selection for double crossover mutants. Plasmid loss was then confirmed by thiamphenicol sensitivity. Single and double toxin mutants, as well as *tcdA* KO was confirmed by PCR amplification and Sanger sequencing of each site (Table 2). After sequence confirmation, the *pyrE* locus of each strain was restored to wildtype as previously described [24].

Whole genome sequencing and mutant confirmation

Whole genome sequencing was performed to confirm the presence and absence of mutations for all strains used in this study (Table 1). Strains were cultured overnight in 3 mL liquid BHIS, then gDNA was extracted using the MasterPure Gram Positive DNA Purification kit

Table 2. Oligonucleotides used in this study.

Primer name	Sequence (5'-3')
Cloning *tcdA* and *tcdB* GTD fragments	
SbfI-tcdA_F	CCTGCAGGgatttaattgatagtttaaaagttatag
AscI-tcdA_R	GGCGCGCCgtatctaaaaatgaacttatctcattgg
SbfI-tcdB_F	CCTGCAGGcagacaacgtctttattcaatcg
AscI-tcdB_R	GGCGCGCCataagtctcctctacatttacagaatagc
Creating *tcdA* knockout cassette	
*tcdA*_LHA_F	gaccgatcgggccccctgcaGTTTTGGAATAGATGGAGGA
*tcdA*_LHA_R	tttgtcaaacatatattttaCATAAAAACCTCCTAGTACTATTAT
*tcdA*_RHA_F	agtactaggaggtttttatgTAAAATATATGTTTGACAAAAA
*tcdA*_RHA_R	tagctaaggattcagaacggAATGAGGGTAACGAATTTAG
Site directed mutagenesis	
*tcdA*_gib_mutant_F	agtatatttaAatgttAatatgcttccagg
*tcdA*_gib_R	aaagtcagacttacactcagtccaaagg
*tcdA*_gib_mutant_R	gcatatTaacatTtaaatatactccgcc
*tcdA*_gib_F	gagtgtaagtctgactttaaatcatttttagcag
Q5_*tcdB*_F	tAatatgttaccaggaatacaacc
Q5_*tcdB*_R	acatTtaaatatacaccaccaacttc
Screening for toxin mutants and *pyrE* repair	
R2_*tcdA*_F	caaaaacacaaaaatacgtgatgaag
R2_*tcdA*_R	cataatacttaatagtaacttaccaggataag
R2_*tcdB*_F	gaattaactttattgtaaaatcaataacttaatctaag
R2_*tcdB*_R	ctataatagagtcttgacttatagatggc
D_*tcdA*_F	gggatagatatcagggctaa
D_*tcdA*_R	gcttgatttataacactgcc
D_*tcdB*_F	tagaaagatggaatttggca
D_*tcdB*_R	tgctctgaagtatatcctgg
R2_*tcdA*_KO_F	ttatataaacctaggaggcg
R2_*tcdA*_KO_R	ttatataaacctaggaggcg
R2_*pyrE*_F	tgtaaaattatgcttagggg
R2_*pyrE*_R	ttataacattaacatggagg

*Uppercase letters denote overhangs for restriction sites or for Gibson assembly. Upper case letters represent single nucleotide mutations for introduction into *tcdA* or *tcdB*.

https://doi.org/10.1371/journal.ppat.1010323.t002

according to manufacturer's protocol (Lucigen). Library preparation and sequencing was performed by the Microbial Genome Sequencing Center (MiGS). Briefly, DNA quality and quantity was assessed with a Qubit fluorometer prior to library preparation using the Illumina DNA Library Prep kit according to manufacturer's protocol. Samples were sequenced on the Illumina NextSeq 2000 platform as paired end 2x150 bp reads to generate 200 Mbp total reads.

Quality control of reads and adapter trimming was performed using instrument software. Each genome underwent *de novo* assembly and annotation using SPAdes and RASTtk, respectively, in PATRIC 3.6.9 [38–40]. Genomes of all strains were aligned to the reference *C. difficile* R20291 genome (NC_013316) [41] using Burrows-Wheeler Aligner (BWA-mem), then single nucleotide variants and indels were analyzed using FreeBayes in PATRIC 3.6.9 [40,42,43]. Finally, *tcdA* and *tcdB* genes from all strains were aligned and presented using Clustal Omega [44]. Sequencing reads were deposited to NCBI Sequencing Read Archive accession number: PRJNA762329.

C. difficile toxin secretion *in vitro*

Immunoblotting of *C. difficile* culture supernatants was used to test toxin secretion in the wild-type and mutant strains. All strains were grown for 18 hours in 3mL liquid BHIS from glycerol stocks. Optical density at 600 nm (OD_{600}) was then measured, and each culture was diluted to OD_{600} = 0.1 in 3 mL of Tryptone Yeast (TY) medium and grown for 18 hours to OD_{600} = 1. Bacterial suspensions were centrifuged at 3,220 x g for 15 minutes at 4˚C, then the supernatants were filtered through a 0.2 μm cellulose acetate membrane (VWR) into sterile 15 mL conical tubes. One hundred microliters of supernatant suspensions were transferred to tubes containing 50 μl 2x Laemmli buffer and β-mercaptoethanol then heated at 90˚C for 5 min. Twenty-five microliters of 6x loading dye were added to each tube, and 50 μl of each suspension were loaded into two sodium dodecyl sulphate-polyacrylamide stain-free gels (SDS-PAGE; 4–20% Mini-PROTEAN TGX Stain-Free Protein Gels, Bio-Rad) and run at 150 V for one hour. Gels were gently rinsed in milliQ water and total protein was imaged on a Bio-Rad Gel Doc EZ System by exposing to UV light for 2.5 min.

Proteins were transferred from the SDS-PAGE gels to polyvinylidene fluoride membranes at 100 V for 1 hour. The membranes were then transferred to individual containers and blocked in 5% milk in tris buffered saline pH 7.6 supplemented with 0.1% Tween 20 (TBST) for 30 minutes at 4˚C. After blocking, the solution was removed, and the membranes were incubated in TBST-5% milk containing the anti-TcdB-GTD antibody, 20B3, at a 1:1000 dilution, or anti-TcdA antibody (clone PCG4.1, Novus Biologicals) at a 1:1000 dilution overnight at 4˚C [12,45]. The next day, the membranes were washed three times in TBST then incubated with anti-mouse IgG (H+L) DyLight 680 Conjugate (Cell Signaling) diluted 1:10,000 in TBST-5% milk solution for 1 hour at room temperature. The membranes were washed three times in TBST and imaged in the 700nm wavelength channel on a Li-Cor Odyssey. This experiment was performed three times. Densitometry measurements were performed in FIJI by normalizing Western band intensity to total protein from the stain-free gel images. Graphs were generated using ggplot2, and statistical differences between groups were assessed using one-way ANOVA and Tukey's HSD in R v. 4.0.3.

C. difficile growth *in vitro*

Strain growth in artificial media was measured to test differences in growth rate *in vitro*. Briefly, each strain was plated on BHIS from glycerol stocks, then grown overnight as described above. Five CFUs from each strain were transferred into 3 mL BHIS and grown statically for 18 hours. The next day, cultures were diluted to OD_{600} = 0.05 in wells of a 96-well plate (Nunc) containing 200 μl BHIS. Control mock-inoculated wells were included by adding sterile PBS into six wells. OD_{600} was measured every hour for 24 hours in a BioTek Synergy 4 microplate reader (BioTek-Agilent). *In vitro* growth graphs were generated using ggplot2 and ggprism, and statistical differences between groups at each timepoint were assessed by calculating and plotting the 95% confidence interval in R v. 4.0.3.

Cell rounding assays

Vero cells (ATCC CCL-81; cultured in DMEM, 10% fetal bovine serum, 5% CO_2) were seeded in a black 96-well plate at a concentration of 20,000 cells per well and incubated overnight. *C. difficile* supernatants were obtained from toxin-inducing TY medium at OD_{600} = 1 exactly as described above. Wildtype recombinant TcdA (VPI 10463) and TcdB (R20291) were expressed and purified as previously described [46]. Bacterial supernatants, purified TcdA and TcdB, and TY were diluted 10-fold and 200 μl of each sample was placed in individual wells in technical duplicate and plates were statically incubated in a BioTek Cytation 5 plate reader at 37˚C

with 5% CO_2, where brightfield images were acquired every hour for 10 hours. This experiment was performed three times. The number of rounded cells versus number of total cells per image was analyzed for 1:100 dilutions of bacterial supernatants and TY, or concentrations of 100 pM TcdA and 1 pM TcdB at selected timepoints in FIJI. Graphs were generated using ggplot2, and statistical differences between groups were assessed using one-way ANOVA and Tukey's HSD in R v. 4.0.3.

Mouse model of *C. difficile* infection

Differences in virulence between mutant and wildtype strains were tested using the cefoperazone mouse model of *C. difficile* infection [18]. Nine-week-old C57BL/6J female mice were treated with cefoperazone (0.5 mg/kg) in sterile drinking water *ad libitum* for five days, followed by two days of untreated water prior to inoculation [18]. Mice were inoculated with 10^5 CFU/mL spores in 100 μl of sterile PBS via transoral gastric gavage.

Mouse weight and symptoms were recorded daily, and daily stool samples were collected. Stool samples were scored on a 1–4 scale for color and composition as an additional metric of disease, where 1 = normal, well-formed stool; 2 = well-formed, discolored stool; 3 = moist, soft, and discolored stool; and 4 = wet tail, watery diarrhea, and empty cecum & colon. Stool was then weighed, macerated in 500 μl sterile PBS pH 7.4, and 5-fold dilution plated on TA (10% w/v), D-cycloserine (10 mg/mL), cefoxitin (10 mg/mL), and fructose agar (TCCFA) semi-selective media to enumerate *C. difficile* titers *in vivo*. Weight loss, stool score, and daily CFU g^{-1} graphs were plotted with ggplot2 and ggprism, and statistical differences at each timepoint were tested using one-way ANOVA and Tukey's HSD test (weight loss) or Kruskal-Wallis and Dunn's test (CFU g^{-1} stool) in R v. 4.0.3.

Mice were humanely euthanized at two- or four-days post-inoculation by CO_2 inhalation. Post-sacrifice, the colon and cecum were excised from each animal and imaged to measure size. After imaging, the whole colon was flushed with sterile PBS, cut transversally, then splayed open and fixed in 2% paraformaldehyde (PFA) at 4˚C for 2 hours. Intact ceca were laid flat on sterile Whatman filter paper and fixed in 2% PFA for two hours at 4˚C. After fixation, tissues were washed three times in cold, sterile PBS, then transferred to an ice-cold solution of 30% sucrose, 1% sodium azide and incubated for 16 hours at 4˚C. Tissues were then embedded in OCT (Optimal Cutting Temperature embedding medium; Fisher Healthcare) on dry ice-cooled ethanol and stored at -80˚C until use. Images were used to determine the length of colons and area of ceca (n = 6 per treatment) using ImageJ. These metrics were graphed using ggplot2 and ggprism, and statistical differences were determined using one-way ANOVA and Tukey's HSD test in R v. 4.0.3.

Histopathological assessment

Frozen tissue blocks of ceca and colons were sectioned on a Leica CM1950 Cryostat (Leica Biosystems) as 7 μm slices onto Superfrost Plus microscope slides (Fisher Scientific) and stored at -80˚C until use. To assess histopathology, cecum sections were stained with hematoxylin & eosin (H&E; Vector Labs), and conditions were masked for a board-certified gastrointestinal pathologist to score edema, inflammation, and epithelial damage based on published criteria (n = 6–9 per treatment) [18]. Histological scores were graphed with ggplot2 and ggprism, and statistical differences were determined using one-way ANOVA and Tukey's HSD test in R v. 4.0.3. Presented images were captured using a Leica SCN400 Slide Scanner automated digital image system from Leica Microsystems at the Digital Histology Shared Resource (DHSR) at VUMC. Whole slides were imaged at 40x magnification to a resolution of 0.25 μm/pixel.

Assessment of myeloperoxidase-positive immune cell recruitment during infection

Immune cell infiltration was detected by anti-myeloperoxidase (MPO) staining performed at the VUMC Translational Pathology Shared Resource. Briefly, slides were placed on the Leica Bond RX IHC stainer. Slides were placed in a Protein Block (DAKO) for 10 minutes, then incubated with anti-MPO (DAKO A0398) for one hour at 1:4000 dilution. The Bond Polymer Refine detection system was used for visualization. Slides were then dehydrated, cleared and coverslipped. To quantify immune cell infiltrates, a single mucosal layer was visualized in a 20x field of view (FOV) at a time, and the number of MPO^+ cells were counted per FOV in that region. The number of MPO^+ cells was quantified in three FOVs per mouse per treatment. The average MPO^+ cells per mouse per treatment ($n = 3$) were plotted using ggplot2 and ggprism, and differences were tested using one-way ANOVA and Tukey's HSD test in R v. 4.0.3. Presented images were captured using a Leica SCN400 Slide Scanner at the VUMC DHSR as described above.

Supporting information

S1 Fig. Confirmation of mutant glucosyltransferase phenotypes in cell rounding assays. (A & B). Supernatants of *C. difficile* strains, purified recombinant TcdA (100 pM), TcdB (1 pM), tryptone-yeast (TY) medium, and Dulbecco's Modified Eagle Medium (DMEM) were used to functionally characterize SNMs and knockout mutations affecting TcdA and/or TcdB *in vitro*. **(A)** Each point is the percentage of rounded Vero cells ($n = 3$ independent experiments) that have undergone toxin-mediated cytopathic changes, and bars represent group means at each hour post-intoxication. Error bars denote standard error of the mean. Significantly different groups as determined by Tukey's HSD are shown as letters, where groups containing multiple letters are not significantly different to individuals containing those single letters ($p < 0.05$). **(B)** Representative images of Vero cells after 0- or 10-hours post-inoculation with each individual treatment.
(TIF)

S2 Fig. Percent weight loss from day 0 weight during infection studies. Positive increases signify weight lost and negative decreases indicate weight gained. Each point is an individual animal and bars represent group means at each day. Error bars denote standard error of the mean. Significantly different groups as determined by Tukey's HSD test are shown using letters where groups containing multiple letters are not significantly different to individuals containing those single letters ($p < 0.05$).
(TIF)

Acknowledgments

Thank you to Melissa Farrow and members of the Lacy lab for stimulating discussions and feedback on these experiments, to Nick Markham and members of the Skaar lab for advice on the mouse model of *C. difficile* infection, and to Grace Morales for advice on genome analyses. Thank you to Nigel Minton for supporting this work by providing lab space and equipment access for Rory Cave.

Author Contributions

Conceptualization: F. Christopher Peritore-Galve, Rory J. Cave, Sarah A. Kuehne, D. Borden Lacy.

Data curation: F. Christopher Peritore-Galve.

Formal analysis: F. Christopher Peritore-Galve, Kevin O. Childress, M. Kay Washington, Sarah A. Kuehne, D. Borden Lacy.

Funding acquisition: F. Christopher Peritore-Galve, D. Borden Lacy.

Investigation: F. Christopher Peritore-Galve, John A. Shupe, Rory J. Cave, M. Kay Washington, Sarah A. Kuehne.

Methodology: F. Christopher Peritore-Galve, John A. Shupe, Rory J. Cave, Kevin O. Childress, M. Kay Washington, Sarah A. Kuehne, D. Borden Lacy.

Project administration: F. Christopher Peritore-Galve, Sarah A. Kuehne, D. Borden Lacy.

Resources: Sarah A. Kuehne, D. Borden Lacy.

Supervision: Sarah A. Kuehne, D. Borden Lacy.

Validation: F. Christopher Peritore-Galve, Rory J. Cave, Sarah A. Kuehne, D. Borden Lacy.

Visualization: F. Christopher Peritore-Galve, Kevin O. Childress, D. Borden Lacy.

Writing – original draft: F. Christopher Peritore-Galve, D. Borden Lacy.

Writing – review & editing: F. Christopher Peritore-Galve, John A. Shupe, Rory J. Cave, Kevin O. Childress, M. Kay Washington, Sarah A. Kuehne, D. Borden Lacy.

References

1. Centers for Disease Control and Prevention, Antibiotic resistance threats in the United States. 2019. https://doi.org/10.15620/cdc:82532.
2. Lessa FC, Mu Y, Bamberg WM, Zintars GB, Dumyati GK, Dunn JR, et al. Burden of *Clostridium difficile* infection in the United States. N. Engl. J. Med. 2015; 372: 825–834. https://doi.org/10.1056/NEJMoa1408913 PMID: 25714160
3. Smits WK, Lyras D, Lacy DB, Wilcox MH, Kuijper EJ. *Clostridium difficile* infection. Nat. Rev. Dis. Primers. 2016; 2: 1–20. https://doi.org/10.1038/nrdp.2016.20 PMID: 27158839
4. Smith AB, Ocana JS, Zackular JP. From nursery to nursing home: emerging concepts in *Clostridioides difficile* pathogenesis. Infect. Immunol. 2020; 88: 7. https://doi.org/10.1128/IAI.00934-19 PMID: 32122939
5. Chandrasekaran R, Lacy DB. The role of toxins in *Clostridium difficile* infection. FEMS Microbiol. Rev. 2017; 41: 723–750. https://doi.org/10.1093/femsre/fux048 PMID: 29048477
6. Genisyuerek S, Papatheodorou P, Guttenberg G, Schubert R, Benz R, Aktories K. Structural determinants for membrane insertion, pore formation and translocation of *Clostridium difficile* toxin B. Mol. Microbiol. 2011; 79: 1643–1654. https://doi.org/10.1111/j.1365-2958.2011.07549.x PMID: 21231971
7. Just I, Selzer J, Wilm M, von Eichel-Streiber C, Mann M, Aktories K. Glucosylation of Rho proteins by *Clostridium difficile* toxin B. Nature. 1995; 375: 500–503. https://doi.org/10.1038/375500a0 PMID: 7777059
8. Just I, Wilm M, Selzer J, Rex G, von Eichel-Streiber C, Mann M, Aktories K. The enterotoxin from *Clostridium difficile* (ToxA) monoglucosylates the Rho proteins. J. Biol. Chem. 1995; 270: 13932–13936. https://doi.org/10.1074/jbc.270.23.13932 PMID: 7775453
9. Yu H, Chen K, Sun Y, Carter M, Garey KW, Savidge TC, et al. Cytokines are markers of the *Clostridium difficile*-induced inflammatory response and predict disease severity. Clin. Vaccine Immunol. 2017; 24: e00037–17. https://doi.org/10.1128/CVI.00037-17 PMID: 28592627
10. El Feghaly RE, Stauber JL, Deych E, Gonzalez C, Tarr PI, Haslam DB. Markers of intestinal inflammation, not bacterial burden, correlate with clinical outcomes in *Clostridium difficile* infection. Clin. Infect. Dis. 2013; 56: 1713–1721. https://doi.org/10.1093/cid/cit147 PMID: 23487367
11. Abhyankar MM, Ma JZ, Scully KW, Nafziger AJ, Frisbee AL, Saleh MM, et al. Immune profiling to predict outcome of *Clostridioides difficile* infection. mBio 2020; 11: e00905–20. https://doi.org/10.1128/mBio.00905-20 PMID: 32457246

12. Chumbler NM, Farrow MA, Lapierre LA, Franklin JL, Haslam DB, Goldenring JR, Lacy DB. *Clostridium difficile* toxin B causes epithelial cell necrosis through an autoprocessing-independent mechanism. PLoS Pathog. 2012; 8: e1003072. https://doi.org/10.1371/journal.ppat.1003072 PMID: 23236283

13. Wohlan K, Goy S, Olling A, Srivaratharajan S, Tatge H, Genth H, Gerhard R. Pyknotic cell death induced by *Clostridium difficile* TcdB: chromatin condensation and nuclear blister are induced independently of the glucosyltransferase activity. Cell. Microbiol. 2014; 16: 1678–1692. https://doi.org/10.1111/cmi.12317 PMID: 24898616

14. Farrow MA, Chumbler NM, Lapierre LA, Franklin JL, Rutherford SA, Goldenring JR, Lacy DB. Clostridium difficile toxin B-induced necrosis is mediated by the host epithelial cell NADPH oxidase complex. Proc. Nat. Acad. Sci. 2013; 110: 18674–18679. https://doi.org/10.1073/pnas.1313658110 PMID: 24167244

15. Chumbler NM, Farrow MA, Lapierre LA, Franklin JL, Lacy DB. *Clostridium difficile* toxins TcdA and TcdB cause colonic tissue damage by distinct mechanisms. Infect. Immun. 2016; 84: 2871–2877. https://doi.org/10.1128/IAI.00583-16 PMID: 27456833

16. Bilverstone TW, Garland M, Cave RJ, Kelly ML, Tholen M, Bouley DM, et al. The glucosyltransferase activity of *C. difficile* Toxin B is required for disease pathogenesis. PLoS Pathog. 2020; 16: e1008852. https://doi.org/10.1371/journal.ppat.1008852 PMID: 32960931

17. Hutton ML, Mackin KE, Chakravorty A, Lyras D. Small animal models for the study of *Clostridium difficile* disease pathogenesis. FEMS Microbiol. Lett. 2014; 352: 140–149. https://doi.org/10.1111/1574-6968.12367 PMID: 24372713

18. Theriot CM, Koumpouras CC, Carlson PE, Bergin II, Aronoff DM, Young VB. Cefoperazone-treated mice as an experimental platform to assess differential virulence of *Clostridium difficile* strains. Gut Microbes. 2011; 2: 326–334. https://doi.org/10.4161/gmic.19142 PMID: 22198617

19. Kordus SL, Thomas AK, Lacy DB. *Clostridioides difficile* toxins: mechanisms of action and antitoxin therapies. Nat. Rev. Microbiol. 2021; https://doi.org/10.1038/s41579-021-00660-2 PMID: 34837014

20. Voth DE, Ballard JD. *Clostridium difficile* toxins: mechanism of action and role in disease. Clin. Microbiol. Rev. 2005; 18: 247–263. https://doi.org/10.1128/CMR.18.2.247-263.2005 PMID: 15831824

21. Lyras D, O'Connor JR, Howarth PM, Sambol SP, Carter GP, Phumoonna T, et al. Toxin B is essential for virulence of *Clostridium difficile*. Nature. 2009; 458: 1176–1179. https://doi.org/10.1038/nature07822 PMID: 19252482

22. Carter GP, Chakravorty A, Nguyen TAP, Mileto S, Schreiber F, Li L, et al. Defining the roles of TcdA and TcdB in localized gastrointestinal disease, systemic organ damage, and the host response during *Clostridium difficile* infections. mBio. 2015; 6 (3): e00551. https://doi.org/10.1128/mBio.00551-15 PMID: 26037121

23. Kuehne SA, Cartman ST, Heap JT, Kelly ML, Cockayne A, Minton NP. The role of toxin A and toxin B in *Clostridium difficile* infection. Nature. 2010; 467: 711–713. https://doi.org/10.1038/nature09397 PMID: 20844489

24. Ng YK, Ehsaan M, Philip S, Collery MM, Janoir C, Collignon A, et al. Expanding the repertoire of gene tools for precise manipulation of the *Clostridium difficile* genome: allelic exchange using *pyrE* alleles. PLoS ONE. 2013; 8: e56051. https://doi.org/10.1371/journal.pone.0056051 PMID: 23405251

25. Monteford J, Bilverstone TW, Ingle P, Philip S, Kuehne SA, Minton NP. What's a SNP between friends: the lineage of *Clostridioides difficile* R20291 can effect research outcomes. Anaerobe. 2021; 71: 102422. https://doi.org/10.1016/j.anaerobe.2021.102422 PMID: 34343672

26. Farooq PD, Urrunaga NH, Tang DM, von Rosenvinge EC. Pseudomembranous Colitis. Dis. Mon. 2015; 61: 181–206. https://doi.org/10.1016/j.disamonth.2015.01.006 PMID: 25769243

27. Ng J, Hirota SA, Gross O, Li Y, Ulke-Lemee A, Potentier MS, et al. *Clostridium difficile* toxin–induced inflammation and intestinal injury are mediated by the inflammasome. Gastroenterology. 2010; 139: 542–552. https://doi.org/10.1053/j.gastro.2010.04.005 PMID: 20398664

28. Donald RGK, Flint M, Kalyan N, Johnson E, Witko SE, Kotash C, et al. A novel approach to generate a recombinant toxoid vaccine against *Clostridium difficile*. Microbiology. 2013; 159: 1254–1266. https://doi.org/10.1099/mic.0.066712-0 PMID: 23629868

29. Li S, Shi L, Yang Z, Zhang Y, Perez-Cordon G, Huang T, et al. Critical roles of *Clostridium difficile* toxin B enzymatic activities in pathogenesis. Infect. Immun. 2015; 83: 502–513. https://doi.org/10.1128/IAI.02316-14 PMID: 25404023

30. Yang Z, Zhang Y, Huang T, Feng H. Glucosyltransferase activity of *Clostridium difficile* toxin B is essential for disease pathogenesis. Gut Microbes. 2015; 6: 221–224. https://doi.org/10.1080/19490976.2015.1062965 PMID: 26091306

31. Lyerly DM, Saum KE, MacDonald DK, Wilkins TD. Effects of *Clostridium difficile* toxins given intragastrically to animals. Infect. Immun. 1985; 47: 349–352. https://doi.org/10.1128/iai.47.2.349-352.1985 PMID: 3917975

32. Qiu B, Pothoulakis C, Castagliuolo I, Nikulasson S, LaMont JT. Participation of reactive oxygen metabolites in *Clostridium difficile* toxin A-induced enteritis in rats. Am. J. Physiol. Gastrointest. Liver Physiol.1999; 276: G485–G490. https://doi.org/10.1152/ajpgi.1999.276.2.G485 PMID: 9950823

33. Kelly CP, Becker S, Linevsky JK, Joshi MA, O'Keane JC, Dickey BF, et al. Neutrophil recruitment in *Clostridium difficile* toxin A enteritis in the rabbit. J. Clin. Invest. 1994; 93: 1257–1265. https://doi.org/10.1172/JCI117080 PMID: 7907603

34. Pothoulakis C, LaMont JT. Microbes and microbial toxins: paradigms for microbial- mucosal interactions II. The integrated response of the intestine to *Clostridium difficile* toxins. Am. J. Physiol. Gastrointest. Liver Physiol. 2001; 280: G178–G183. https://doi.org/10.1152/ajpgi.2001.280.2.G178 PMID: 11208538

35. Triadafilopoulous G, Pothoulakis C, Weiss R, Giampaolo C, LaMont JT. Comparative study of *Clostridium difficile* toxin A and cholera toxin in rabbit ileum. Gastroenterology. 1989; 97: 1186–1192. https://doi.org/10.1016/0016-5085(89)91689-2 PMID: 2551764

36. Perez J, Springthorpe VS, Sattar SA, Clospore: a liquid medium for producing high titers of semi-purified spores of *Clostridium difficile*. J. AOAC Int. 2011; 94: 618–626. PMID: 21563698

37. Purdy D, O'Keeffe TAT, Elmore M, Herbert M, McLeod A, Bokori-Brown M, et al. Conjugative transfer of clostridial shuttle vectors from *Escherichia coli* to *Clostridium difficile* through circumvention of the restriction barrier. Mol. Microbiol. 2002; 46: 439–452. https://doi.org/10.1046/j.1365-2958.2002.03134.x PMID: 12406220

38. Bankevich A, Nurk S, Antipov D, Gurevich AA, Dvorkin M, Kulikov AS, et al. SPAdes: a new genome assembly algorithm and its applications to single-cell sequencing. J. Comput. Biol. 2012; 19: 455–477. https://doi.org/10.1089/cmb.2012.0021 PMID: 22506599

39. Brettin T, Davis JJ, Disz T, Edwards RA, Gerdes S, Olsen GJ, et al. RASTtk: a modular and extensible implementation of the RAST algorithm for building custom annotation pipelines and annotating batches of genomes. Sci. Rep. 2015; 5: 8365. https://doi.org/10.1038/srep08365 PMID: 25666585

40. Davis JJ, Wattam AR, Aziz RK, Brettin T, Butler R, Butler RM, et al. The PATRIC Bioinformatics Resource Center: expanding data and analysis capabilities. Nucleic Acids Res. 2020; 48: D606–D612. https://doi.org/10.1093/nar/gkz943 PMID: 31667520

41. He M, Sebaihia M, Lawley TD, Stabler RA, Dawson LF, Martin MJ, et al. Evolutionary dynamics of *Clostridium difficile* over short and long time scales. Proc. Nat. Acad. Sci. 2010; 107: 7527–7532. https://doi.org/10.1073/pnas.0914322107 PMID: 20368420

42. Li H, Durbin R, Fast and accurate short read alignment with Burrows-Wheeler transform. Bioinformatics. 2009; 25: 1754–1760. https://doi.org/10.1093/bioinformatics/btp324 PMID: 19451168

43. Garrison E, Marth G. Haplotype-based variant detection from short-read sequencing. arXiv. 2012; arXiv:1207.3907v2 [q-bio.GN].

44. McWilliam H, Li W, Uludag M, Squizzato S, Park YM, Buso N, et al. Analysis tool web services from the EMBL-EBI. *Nucleic Acids Res.* 2013; 41: W597–W600. https://doi.org/10.1093/nar/gkt376 PMID: 23671338

45. LaFrance ME, Farrow MA, Chandrasekaran R, Sheng J, Rubin DH, Lacy DB. Identification of an epithelial cell receptor responsible for *Clostridium difficile* TcdB-induced cytotoxicity. Proc. Nat. Acad. Sci. 2015; 112: 7073–7078. https://doi.org/10.1073/pnas.1500791112 PMID: 26038560

46. Markham NO, Bloch SC, Shupe JA, Laubacher EN, Thomas AK, Kroh HK, et al. Murine intrarectal instillation of purified recombinant *Clostridioides difficile* toxins enables mechanistic studies of pathogenesis. Infect Immun. 2021; 89: e00543–20. https://doi.org/10.1128/IAI.00543-20 PMID: 33468584

47. Kuehne SA, Minton NP, ClosTron-mediated engineering of Clostridium. Bioengineered. 2012; 3: 247–254. https://doi.org/10.4161/bioe.21004 PMID: 22750794